Supporting Information

Thiophene End-Capped Centrally Extended Acceptor Enables Organic Solar Cells With Efficiency Over 19.3%

Kaihuai Tu,‡[a, b] Xue Jiang,‡[a, b] Gengsui Tian,[a] Lei Liu,[a, b] Yao Chen,[a] Peihao Huang,[a] Chen Chen,[a, b] Hong liang Lei,[a] Tainan Duan *[a] and Zeyun Xiao *[a]

Content:

1. Materials and measurements 2
2. Synthetic Protocols and Characterizations 4
3. Density Functional Theory (DFT) Calculations 6
4. Thermogravimetric Analysis (TGA) 7
5. UV-Vis Spectroscopy 8
6. Contact angle 9
7. OSCs 10
8. Atomic Force Microscopy (AFM) Imaging 11
9. GIWAXS 12
10. Supporting table 13
11. Supporting figure 15
Reference 18

1. Materials and measurements

All commercial chemicals (from *Sigma-Aldrich, Solarmer Energy Inc, Adamas, Alfa Aesar, TCI Chemical Co., Liaoning Youxuan New Energy Technology Co. Ltd* and *Energy Chemical*) were used as received. All reactions and manipulations were carried out under argon atmosphere with the use of standard Schlenk techniques. All these solvents used here were commercially available from Chongqing Chuandong Chemical.Proton nuclear magnetic resonance (^{1}H-NMR) and carbon-13 nuclear magnetic resonance (^{13}C-NMR) spectra of CH-TCl were recorded at 600 MHz and 150 MHz on a Bruker Avance III Ultra shield Plus.MALDI-TOF-TOF were determined on a Bruker Ultraflextreme mass spectrometer.

Calculations: The molecular geometries were optimized by Gaussian 09 with a functional of B3LYP and a basis set of 6-31G(d).[1] The long alkyl chains were replaced by methyl or isobutyl groups to save time.

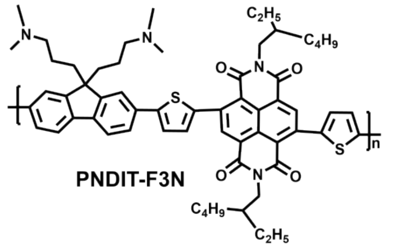

Figure S1. Chemical structure of PNDIT-F3N

Solar cells: OSCs use conventional device configuration as ITO/BrDECz[2]/active blend/PNDIT-F3N/Ag. After cleaning with deionized water, acetone, and isopropanol, the ITO glass was treated with UV-Ozone for 15 minutes.the BrDECz (0.4 mg/mL in ethanol) solution was applied directly onto the ITO substrate for 20 s followed by a spin-coating step at 3000 rpm for 10 s, then placed the ITO substrate onto a hotplate and annealed at 100 °C for 5 min.The PM6:BTP-eC9 (1:1.2 w/w) was dissolved in chloroform at the total blendconcentration of 17 mg/mL with 11 mg/ml 1,4-diiodobenzene (DIB) as the solid additive.The PM6:CH-TCl (1:1.2 w/w) was dissolved in chloroform at the total blend concentration of 17 mg/mL with 11 mg/ml DIB. The PM6:BTP-eC9:CH-TCl (1:1.2:0.1 w/w/w) was dissolved in chloroform at the total blend concentration of 17 mg/mL with 11 mg/ml DIB. All the solutions need to be stirred at a 50 °C for 2 hours to ensure proper dissolution. The blended solution was spin-coated on the BrDECz layer at 3000 rpm for 30 s. It was then annealed at 90 °C for 5 minutes. Then PNDIT-F3N (0.5 mg/mL in methanol added 0.5% acetic acid, 2000 rpm) spin-coated on the active layer, the devices were finally transferred to the evaporation tank to deposit 100 nm Ag. The active area with calibration was 0.1 cm^2.

Electrochemical cyclic voltammogram(CV): CV data was conducted using CIH660e electrochemical workstation with glassy carbon working electrode, platinum wire auxiliary electrode, and Ag/Ag+ glass electrode used as the reference electrode. Ag/Ag$^+$ reference electrode was utilized ferrocene/ferrocenium (Fc/Fc$^+$) redox couple with Fc/Fc$^+$ set relative to 4.8 eV vacuum level. All CV curves were obtained through casting thin films on a glassy carbon electrode.Thermogravimetric analysis data were obtained from a Pyris6 (*PerkinElmer*).

UV-visible (UV-vis) absorption: UV-visible spectra were recorded on a PerkinElmer LAMBDA 365 UV-Vis spectrophotometer.

Contact angle measurement: Contact angles of two solvents (water and formamide) were measured on DSA-100 liquid droplet on the pure film (donor/acceptor) using a shape analysis instrument (KRÜSS Scientific). Miscibility of the two components in the mixture could be estimated based on the solubility parameters (δ) of each material, calculated using the formula: $\delta = K\sqrt{\gamma}$ where γ is the surface energy of the material, and K is a proportionality constant ($K=116 \times 10^3\ m^{1/2}$).

atomic force microscopy (AFM): Topographic images of the films were obtained from a Bruker AFM with the type of dimension edge with Scan AsystTM in the tapping mode using an etched silicon cantilever at a nominal load of ~40nN, and the scanning rate for a 2 μm×2 μm image size was 1.5 Hz.

GIWAXS: GIWAXS measurements were carried out with a Xeuss 2.0 SAXS laboratory beamline using a Cu X-ray source (8.05 keV, 1.54 Å) and a Pilatus3R 300K detector. The incidence angle is 0.2°.

SCLC: The carrier mobility (hole and electron mobility) of photoactive layer was determined by fitting the dark current of hole/electron-only diodes to the space-charge-limited current (SCLC) model. Hole-only diode configuration: ITO/BrDECz/active layer/MoO_3/Ag; Electron-only diode configuration: ITO/ZnO/PNDIT-F_3N/active layer/PNDIT-F_3N/Ag. V_{bi}=0 was used for both fittings. The active layer thickness was determined by a Tencor surface profilometer. The electric-field dependent SCLC mobility was estimated using the following equation[3]:

$$J(V) = \frac{9}{8} e_0 e_r m_0 exp\left(0.89b\sqrt{\frac{V-V_{bi}}{L}}\right)\frac{\left(V-V_{bi}\right)^2}{L^3}$$

Equation 1

2. Synthetic Protocols and Characterizations

M1[4] and M2[5] were synthesized according to the procedure reported in the literature.

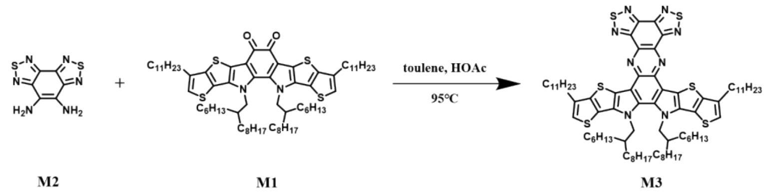

Synthesis of M3: In a round-bottom flask, compound M1 (200mg, 1.0 equiv.) and M2 (46mg, 1.2 equiv.) were dissolved in a mixture solvent (20 mL, toluene: acetic acid=4:1). The reaction mixture was heated to 95 °C and stirred for 24 h. Next, the mixture was concentrated under reduced pressure. The crude product was purified by column chromatography over SiO_2 using hexanes/CH_2Cl_2 (5:1) as the eluent, affording desired compound M3 (163mg, 70%). ^{1}H NMR (600 MHz, Chloroform-d) δ 7.07 (s, 2H), 4.72 (d, J = 7.9 Hz, 4H), 2.90 (t, J = 7.8 Hz, 4H), 2.18 (m, 2H), 1.94-1.88 (m, 4H), 1.50-0.85 (m, 86H), 0.74 (t, J = 7.3 Hz, 6H), 0.66 (t, J = 7.2 Hz, 6H). ^{13}C NMR (151 MHz, Chloroform-d) δ 155.57, 149.02, 144.11, 138.02, 137.28, 136.90, 136.44, 132.43, 123.55, 123.28, 119.70, 117.72, 55.39, 38.92, 32.08, 31.93, 31.75, 30.64, 30.57, 29.87, 29.84, 29.81, 29.71, 29.66, 29.55, 29.52, 29.50, 29.25, 29.12, 25.67, 22.85, 22.70, 22.57, 14.27, 14.18, 14.09.

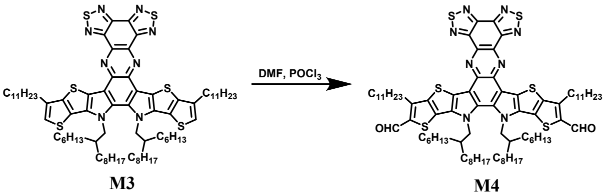

Synthesis of M4: In a pre-dried roundbottom flask, compound M3 (150mg, 1.0 equiv.) , $POCl_3$ (2.0 ml) and DMF (4.0 ml) were dissolved in anhydrous 1,2-dichloroethane (25 mL). The reaction mixture was heated to 90 °C and was stirred for 24 h. Next, the mixture was cooled down and quenched with 3M NaOAc solution (70 mL). The mixture was extracted with $CHCl_3$ (3×50 mL), and the organic phase was combined, dried over Na_2SO_4, filtered, and concentrated under reduced pressure. The crude product was purified by column chromatography over SiO_2 using hexanes/CH_2Cl_2 (3:1) as the eluent to yield the pure dialdehyde M4 (140mg, 90%). ^{1}H NMR (600 MHz, Chloroform-d) δ 10.18 (s, 2H), 4.74 (d, J = 8.0 Hz, 4H), 3.28 (t, J = 7.8 Hz, 4H), 2.15 (m, 2H), 2.02 – 1.94 (m, 4H), 1.68 – 0.82 (m, 86H), 0.74 (t, J = 7.3 Hz, 6H), 0.66 (t, J = 7.1 Hz, 6H). ^{13}C NMR (151 MHz, Chloroform-d) δ 182.04, 155.06, 149.11, 147.21, 144.93, 137.67, 137.46, 137.12, 137.06, 133.43, 129.54, 127.90, 124.16, 123.62, 118.27, 116.07, 55.64, 39.16, 34.86, 32.06, 32.03, 31.88, 31.75, 31.67, 30.91, 30.60, 30.54, 30.44, 29.83, 29.81, 29.79, 29.74, 29.70, 29.64, 29.59, 29.52, 29.49, 29.47, 29.42, 29.24, 29.08, 28.34, 26.05, 25.64, 22.81, 22.67, 22.56, 14.24, 14.15, 14.06.

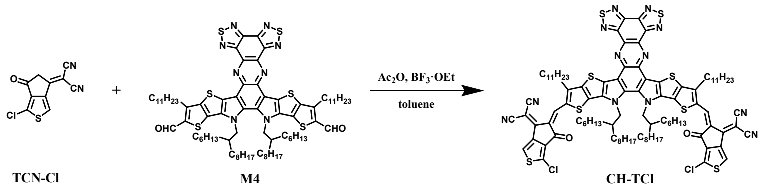

Synthesis of CH-TCl: To a mixed solution of the dialdehyde M4 (100mg, 1.0 equiv.), 2-(1-chloro-6-oxo-5,6-dihydro-4H-cyclopenta[c]thiophen-4-ylidene)malononitrile (42mg, 2.5 equiv.) and acetate anhydride (0.5ml, 20 equiv.) in toluene (20 mL), boron trifluoride etherate (BF3·OEt, 0.2ml, 5 equiv.) was added and the mixture was stirred for 20 min. The reaction mixture was quenched with methanol (50 mL), filtered, and washed with methanol (20 mL) and ethyl acetate (20 mL), affording a black green solid CH-TCl (108mg, 82%) in high purity. Further purification can be simply performed via re-precipitation method. ^{1}H NMR (600 MHz, Chloroform-d) δ 9.10 (s, 2H), 8.18 (s, 2H), 4.94 (d, J = 8.2 Hz, 4H), 3.32 (t, J = 8.1 Hz, 4H), 2.34 (m, 2H), 1.92 (t, J = 8.1 Hz, 4H), 1.62 (d, J = 9.8 Hz, 4H), 1.44–1.04 (m, 76H), 0.88 (t, J = 6.9 Hz, 6H), 0.76-0.68 (m, 12H). ^{13}C NMR (151 MHz, Chloroform-d) δ 180.33, 155.49, 154.36, 154.13, 148.98, 146.85, 141.59, 138.57, 137.11, 136.95, 136.85, 136.37, 136.22, 134.21, 133.86, 131.85, 131.28, 126.83, 125.34, 119.24, 115.19, 66.76, 56.21, 39.74, 32.06, 31.92, 31.89, 31.77, 30.93, 30.12, 30.10, 29.89, 29.84, 29.79, 29.76, 29.55, 29.51, 29.36, 26.15, 26.10, 22.83, 22.71, 22.67, 14.25, 14.16, 14.13.MALDI-TOF MS: calcd. for $C_{100}H_{116}Cl_2N_{12}O_2S_8$ [m/z]: 1844.6594, found 1844.6533

3. Density Functional Theory (DFT) Calculations

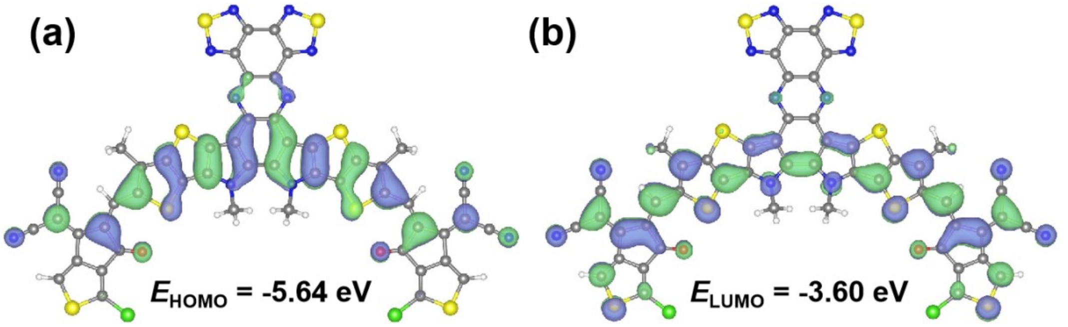

Figure S2. The molecular geometry optimizations of CH-TCl are performed by Gaussian 16[1] at B3LYP/6-31G(d) level, where the long alkyl side chains are simplified to methyl groups for simplifying calculation.

4. Thermogravimetric Analysis (TGA)

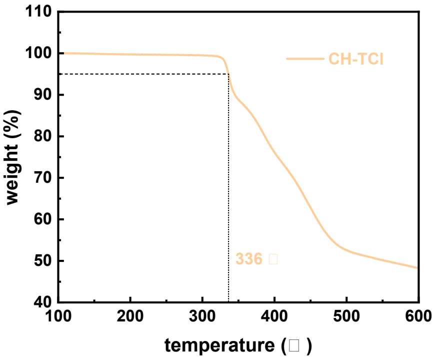

Figure S3. TGA plot with a heating rate of 10 °C/min under N_2 atmosphere, with the temperature for 5% weight loss of CH-TCl being 336.00 °C.

5. UV-Vis Spectroscopy

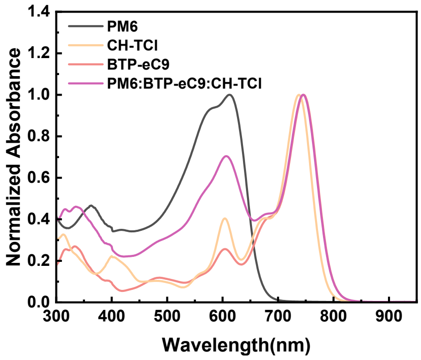

Figure S4. Optical absorption spectra in chloroform solution (normalized absorption spectra)

6. Contact angle

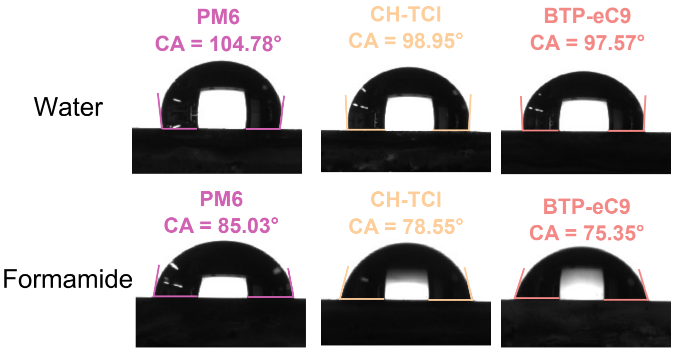

Figure S5. The surface contact angle measurements for the pure films of PM6, CH-TCl, and BTP-eC9. The measurements were carried out by using (a-c) deionized water and (d-f) formamide as wetting liquids.

7. OSCs

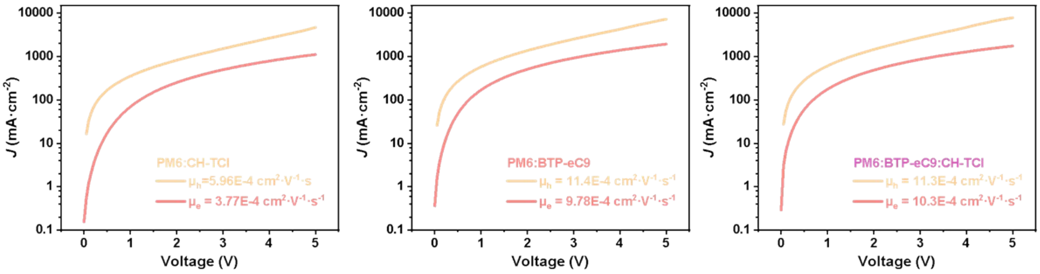

Figure S6. Hole-only devices and electron-only devices of PM6:CH-TCl, PM6:BTP-eC9, and PM6:BTP-eC9:CH-TCl.

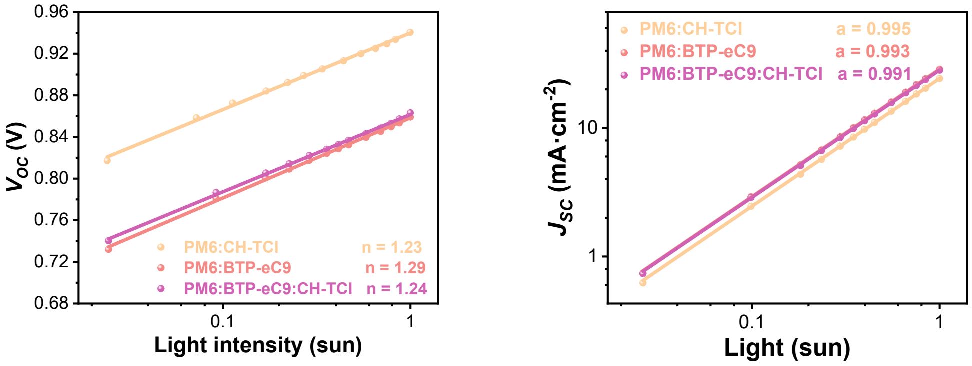

Figure S7. light intensity dependence of V_{OC} and J_{SC}.

8. Atomic Force Microscopy (AFM) Imaging

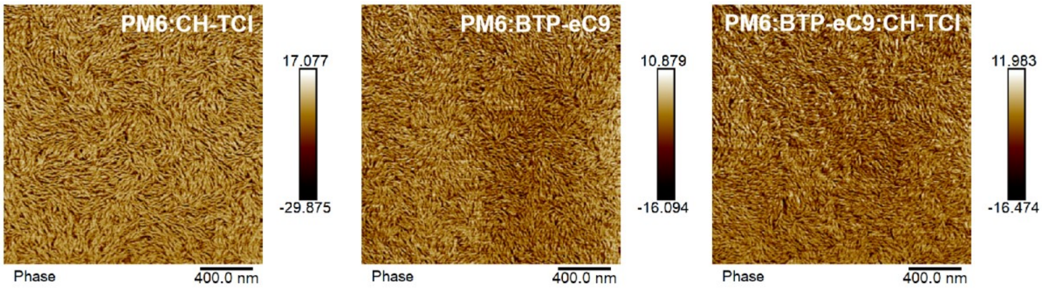

Figure S8. Tapping-mode AFM images depict the phase variations of blend films.

9. GIWAXS

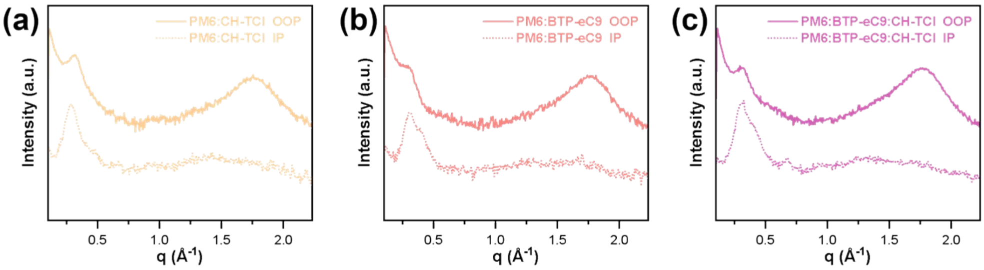

Figure S9. The IP and OOP line-cuts of (a) PM6:CH-TCl, (b) PM6:BTP-eC9, and (c) PM6:BTP-eC9:CH-TCl.

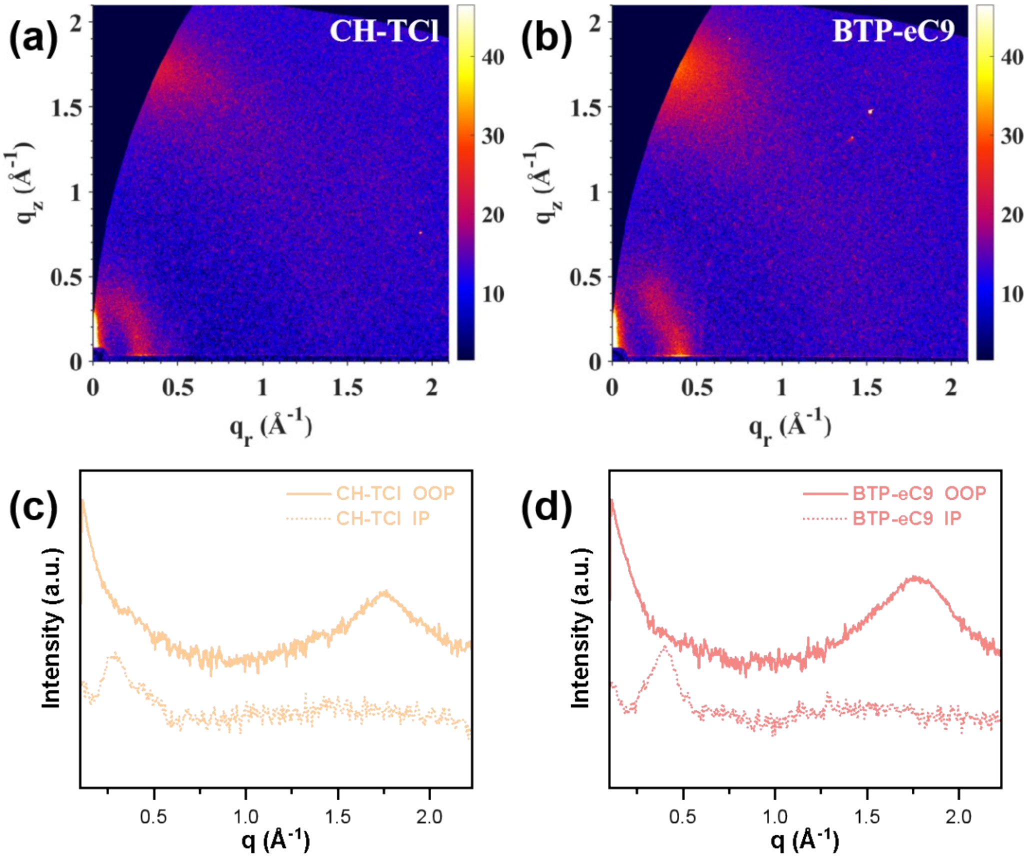

Figure S10. 2D GIWAXS images of (a) CH-TCl, (b) BTP-eC9 films and the corresponding 1D line-cuts in the in-plane and out-of-plane directions of (c) CH-TCl, (d) BTP-eC9, respectively.

10. Supporting table

Table S1. Summary of contact angles (θ), surface energy (γ) and compatibility (c) of PM6, BTP-eC9 and CH-TCl.

Materials	**Contact Angle (water) (°)**	**Contact Angle (FA) (°)**	**surface energy γ (mN/m)**	**χ_{ij} (k)**	
PM6	104.78	85.03	20.18	$\chi_{PM6/CH\text{-}TCl}$	0.1361
CH-TCl	98.95	78.55	23.63	$\chi_{PM6/BTP\text{-}eC9}$	0.4186
BTP-eC9	97.57	75.35	26.41	$\chi_{CH\text{-}TCl/BTP\text{-}eC9}$	0.0773

Table S2. Photovoltaic performances of binary and ternary OSCs based on PM6:BTP-eC9, and PM6:BTP-eC9:CH-TCl photoactive layers(without DIB) with different weight ratios. Other process optimization conditions were mentioned in our previous work.[2]

D:A$_1$:A$_2$	**V_{OC} (V)**	**J_{SC} (mA/cm^2)**	**FF (%)**	**PCE (%)**
1:1.2	0.863	27.82	74.52	17.90
	0.860±0.004	27.72±0.35	73.93±1.85	17.62±0.66
1:1.2:0.05	0.870	28.00	74.60	18.17
	0.868±0.004	27.59±0.52	74.37±1.97	17.83±0.82
1:1.2:0.1	0.873	28.00	75.56	18.46
	0.869±0.004	28.01±0.10	75.04±0.86	18.26±0.19
1:1.2:0.15	0.876	27.92	74.45	18.21
	0.875±0.003	27.70±0.35	74.04±1.48	18.00±0.40

Table S3. Charge carrier mobilities determined by SCLC measurement.

BHJ	**μe (10^{-4} cm^2/Vs)**	**μh (10^{-4} cm^2/Vs)**	**μ_h/μ_e**
PM6:CH-TCl	3.77	5.96	1.58
PM6:BTP-eC9	9.78	11.4	1.17
PM6:BTP-eC9:CH-TCl	10.3	11.3	1.10

Table S4. Crystallographic parameters for the thin films.

Film	**q** **[010, Å-1]**	**d-spacing[a]** **[010, Å]**	**FWHM** **[010, Å^{-1}]**	**CCL[b]** **[010, Å]**
BTP-eC9	1.765	3.56	0.293	19.30
CH-TCl	1.750	3.59	0.254	22.26
PM6:BTP-eC9	1.748	3.59	0.286	19.77
PM6:CH-TCl	1.745	3.60	0.301	18.79
PM6:BTP-eC9:CH-TCl	1.751	3.59	0.285	19.84

[a] Calculated from the equation: d-spacing = $2\pi/q$. [b] Obtained from the Scherrer equation: CCL = 2πK/FWHM, where FWHM is the full-width at half-maximum and K is a shape factor (K = 0.9 here).

11. Supporting figure

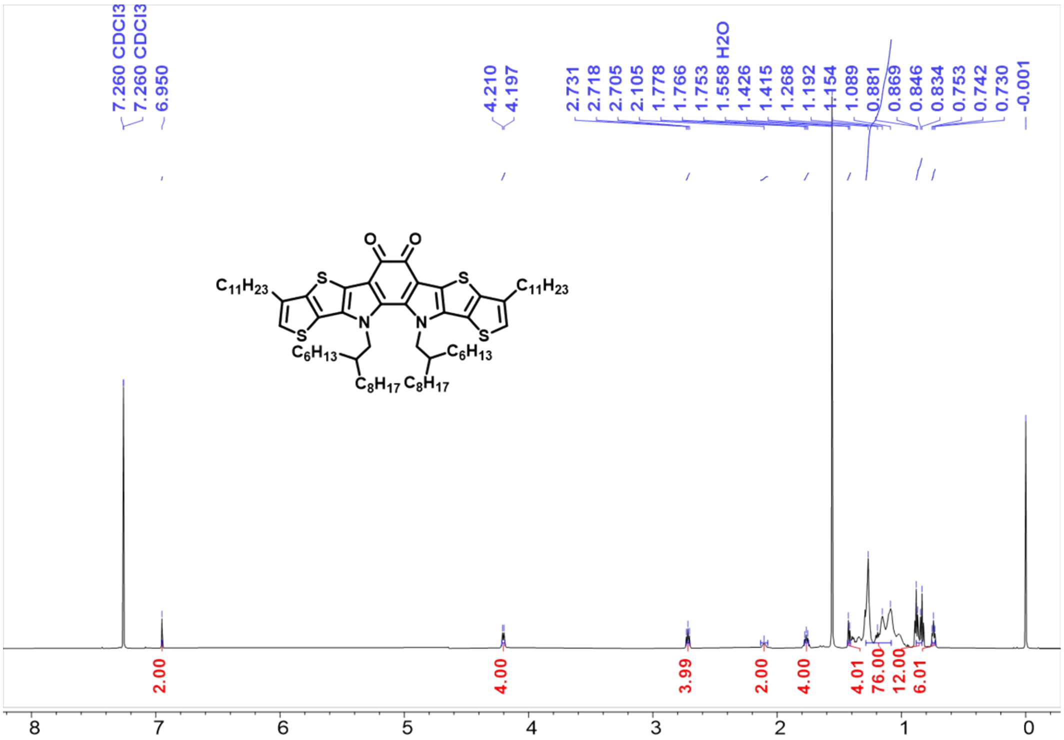

Figure S11. ^{1}H NMR spectrum of **M1** in CDCl$_3$

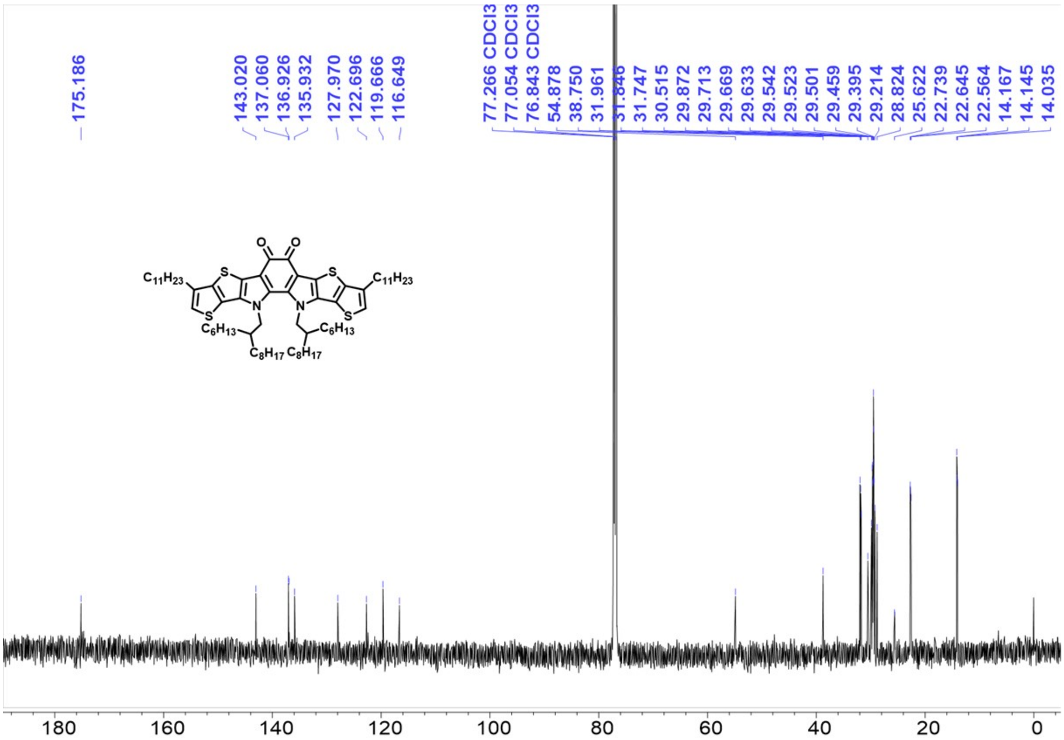

Figure S12. ^{13}C NMR spectrum of **M1** in CDCl$_3$

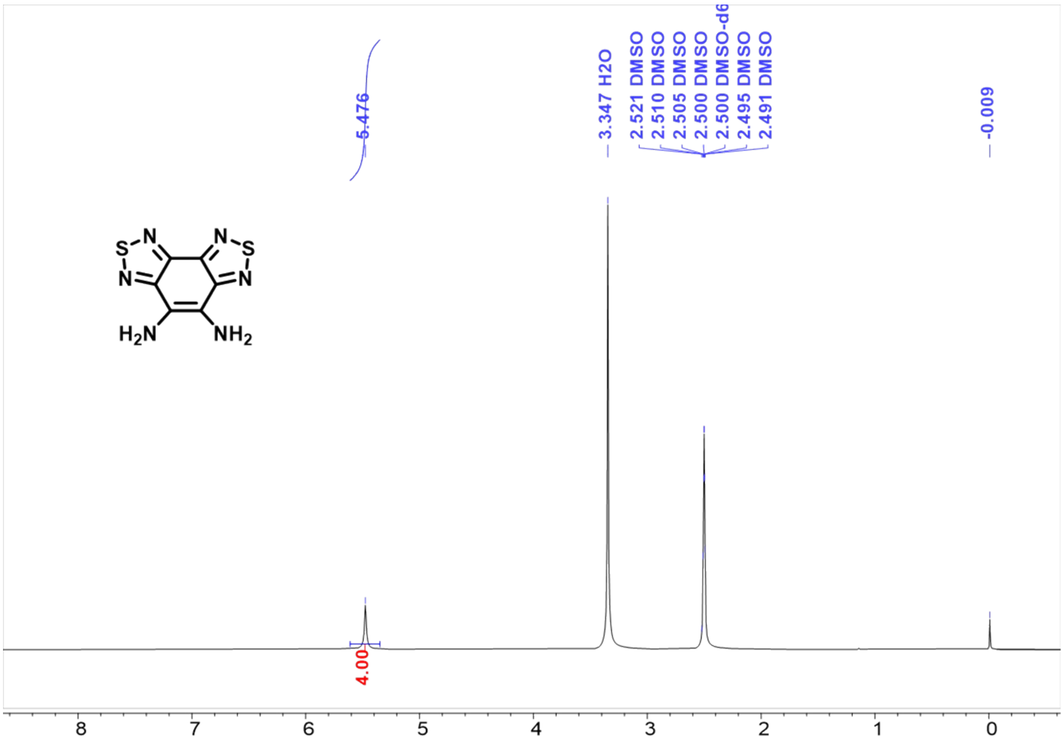

Figure S13. ^{1}H NMR spectrum of **M2** in $CDCl_3$

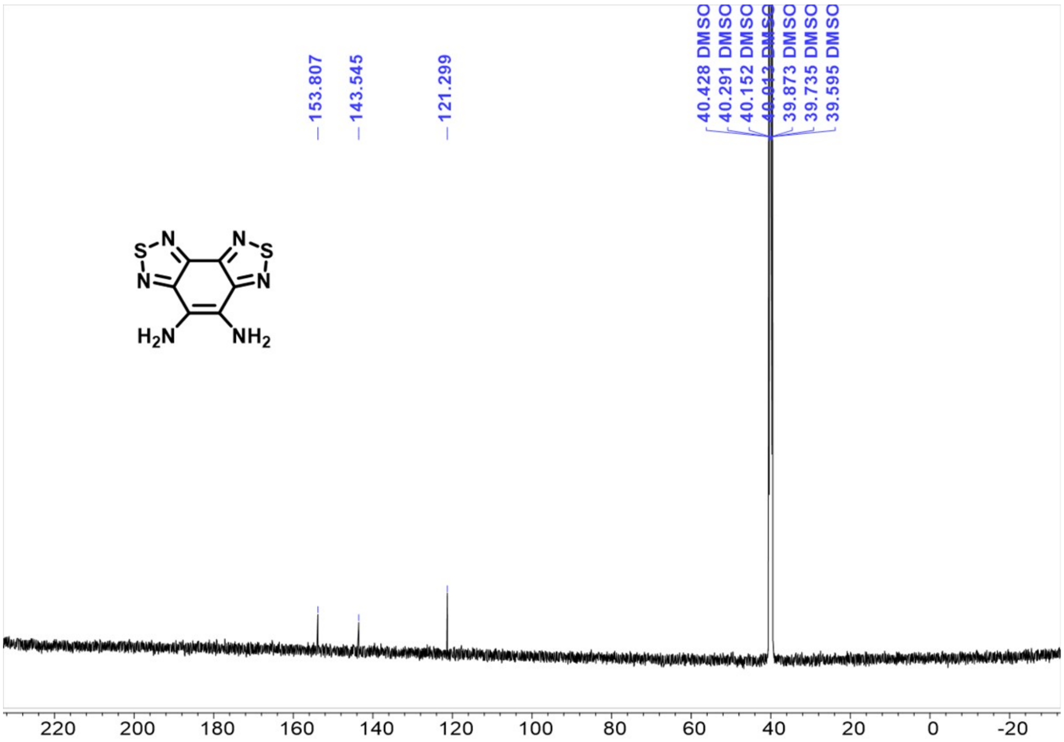

Figure S14. ^{13}C NMR spectrum of **M2** in $CDCl_3$

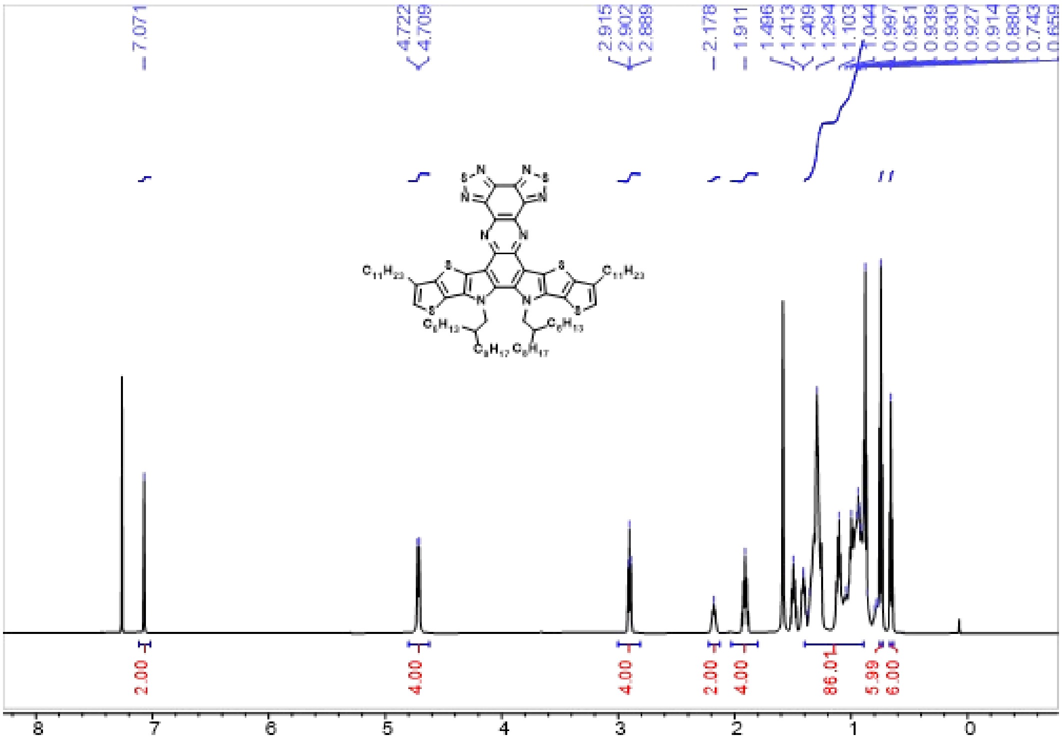

Figure S15. ^{1}H NMR spectrum of **M3** in CDCl$_3$

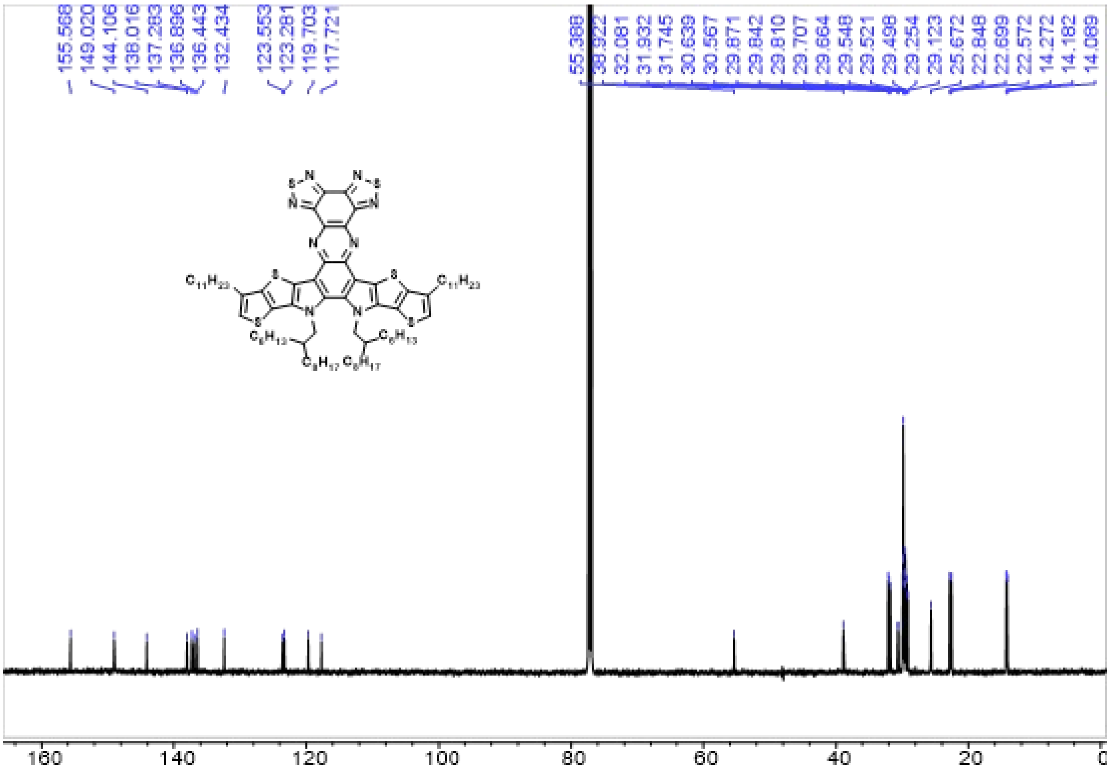

Figure S16. ^{13}C NMR spectrum of **M3** in CDCl$_3$

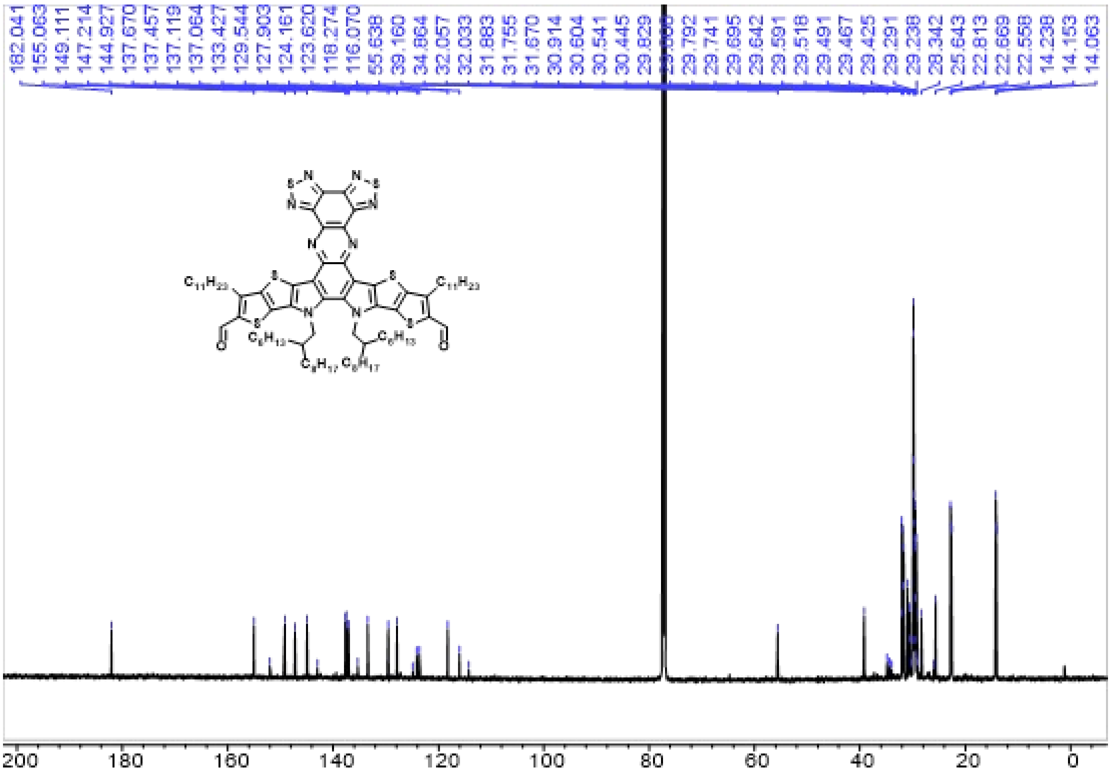

Figure S17. ^{1}H NMR spectrum of **M4** in $CDCl_3$

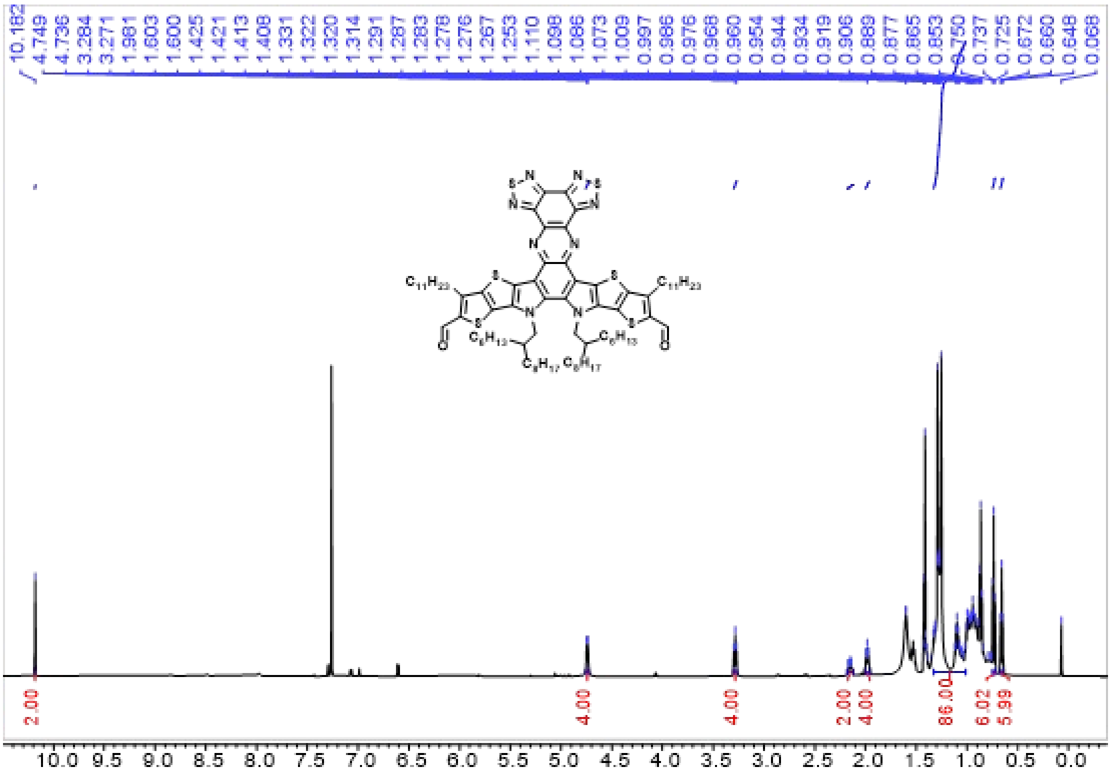

Figure S18. ^{13}C NMR spectrum of **M4** in $CDCl_3$

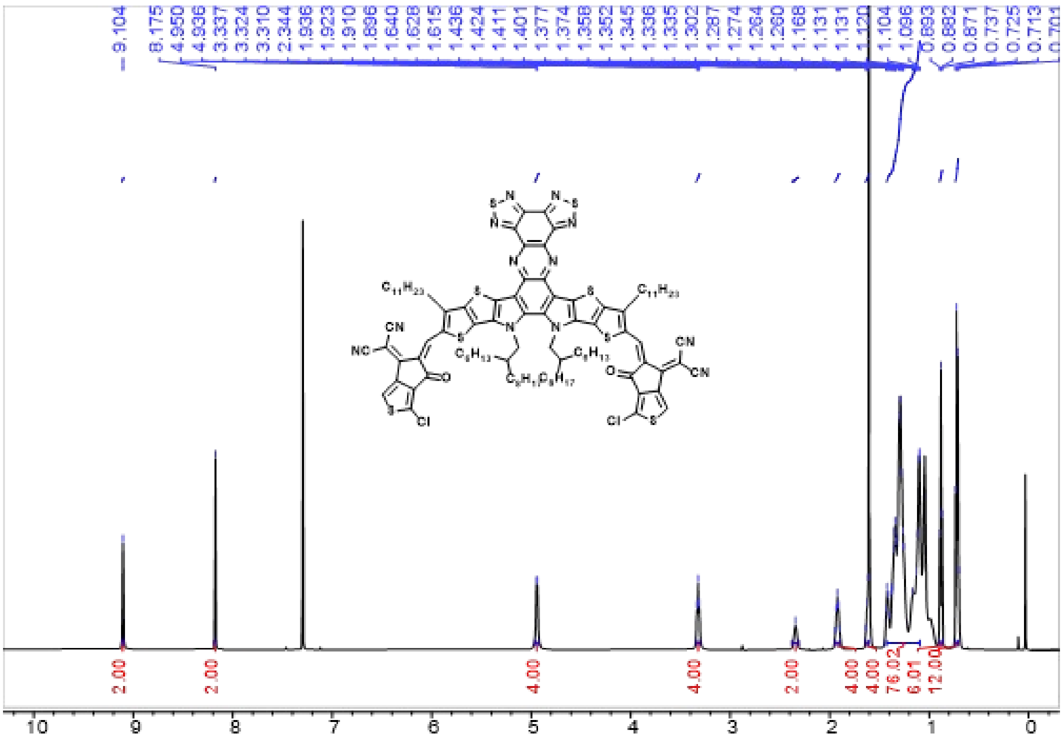

Figure S19. ^{1}H NMR spectrum of **CH-TCl** in $CDCl_3$

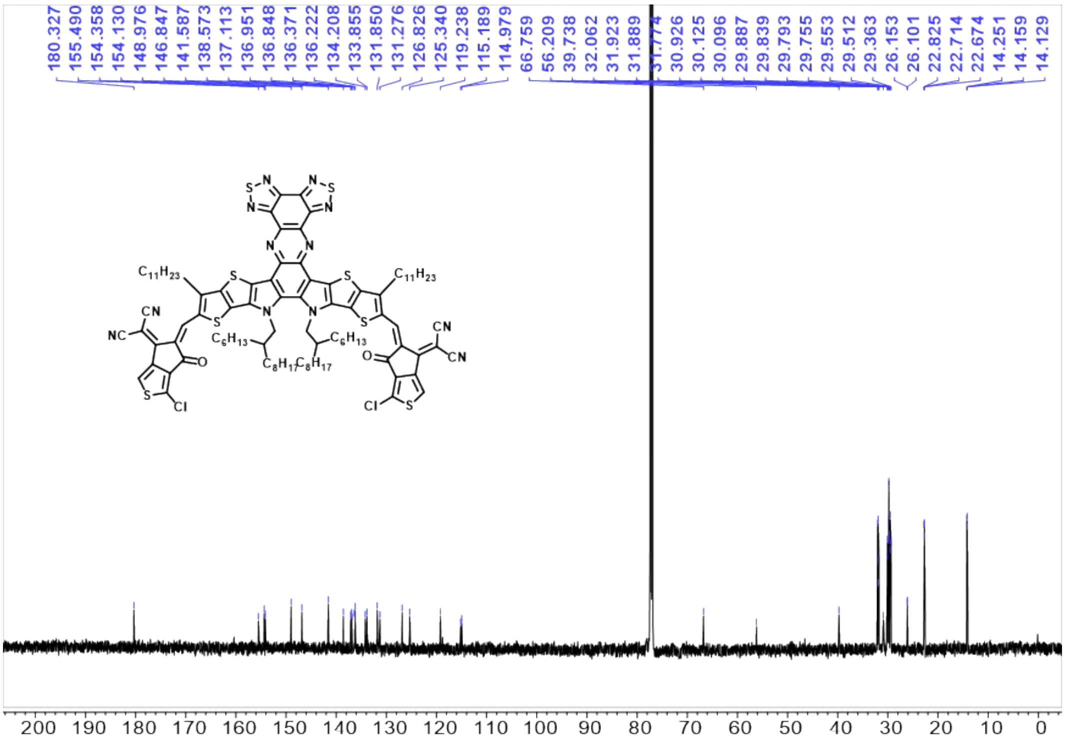

Figure S20. ^{13}C NMR spectrum of **CH-TCl** in $CDCl_3$

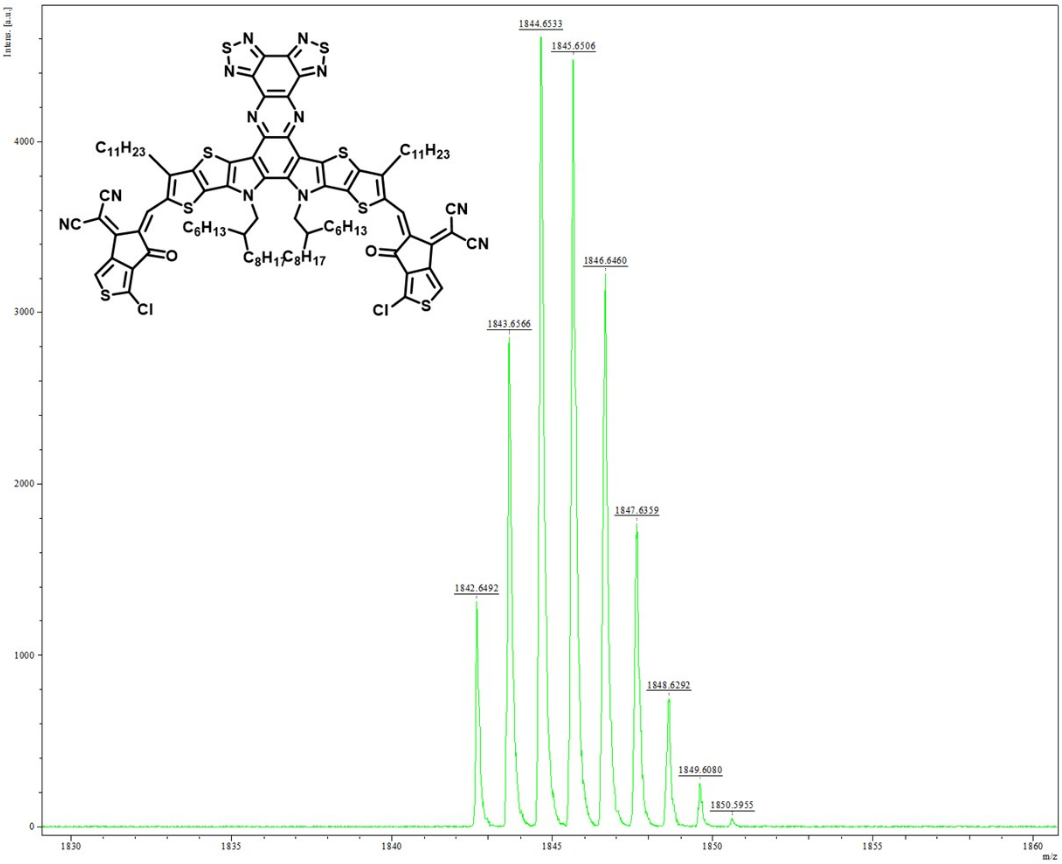

Figure S21. MALDI-TOF spectrum of **CH-TCl**.

Reference

1 M. Frisch, G. Trucks, H. Schlegel, G. Scuseria, M. Robb, J. Cheeseman, G. Scalmani, V. Barone, G. Petersson and H. Nakatsuji, *Gaussian Inc., Wallingford CT*, 2016.

2 L. Liu, F. Yu, H. Dingqin, X. Jiang, P. Huang, Y. Li, G. Tian, H. Lei, S. Wu, K. Tu, C. Chen, T. Gu, Y. Chen, T. Duan and Z. Xiao, *Energy Environ. Sci.*, 2025. DOI: 10.1039/D4EE04515G.

3 D. Hu, H. Tang, S. Karuthedath, Q. Chen, S. Chen, J. I. I. Khan, H. Liu, Q. Yang, J. Gorenflot, C. E. E. Petoukhoff, T. Duan, X. Lu, F. Laquai and S. Lu, *Adv. Funct. Mater.*, 2023, **33**. 2211873.

4 T. Duan, W. Feng, Y. Li, Z. Li, Z. Zhang, H. Liang, H. Chen, C. Zhong, S. Jeong, C. Yang, S. Chen, S. Lu, O. A. Rakitin, C. Li, X. Wan, B. Kan and Y. Chen, *Angew. Chem.-Int. Edit.*, 2023, **62**. e202308832.

5 A. P. Komin and M. Carmack, *J. Heterocycl. Chem.*, 1975, **12**, 829-833.